

The pH Dependence of Ultrafast Charge Dynamics in Graphene Oxide Dispersions

Georgia Kime^{1,2}, Kai-Ge Zhou^{3,4}, Samantha J. O. Hardman⁵, Rahul R. Nair^{3,4}, Konstantin Sergeevich Novoselov², Daria V. Andreeva⁶, and David J. Binks^{1,2*}

¹ Photon Science Institute, University of Manchester, M13 9PL, UK

² School of Physics and Astronomy, University of Manchester, M13 9PL, UK

³ School of Chemical Engineering & Analytical Science, Univ. of Manchester, M13 9PL, UK

⁴ National Graphene Institute, University of Manchester, M13 9PL, UK

⁵ Manchester Institute of Biotechnology, University of Manchester, M13 9PL, UK

⁶ Department of Materials Science and Engineering, National University of Singapore, Singapore, 117575, Singapore

*To whom correspondence should be addressed

ABSTRACT The pH dependence of emission from graphene oxide is believed to be due to the protonation of surface functional groups. In this study we use transient absorption spectroscopy to study the sub-picosecond charge dynamics in graphene oxide over a range of pH values, observing dynamics consistent with an excited state protonation step for pH < 9.3. The timescale of this process is ~ 1.5 ps, and a corresponding change in recombination dynamics follows. A broad photo-induced absorption peak centred at 530 nm associated with excited state protonation is also observed.

Email: david.binks@manchester.ac.uk

1. INTRODUCTION

Graphene oxide (GO), which is often used as a precursor for the chemical synthesis of graphene¹, has gained interest itself due to its photoluminescence (PL) properties and biocompatibility. The mechanisms behind GO PL are particularly interesting as they differ from those found in 2D semiconductors with visible optical band-gap emission such as transition metal dichalcogenides^{2,3}. Functionalization of graphene to form graphene oxide creates a band-gap, but this gap is small (~ 0.6 eV⁴), yet GO emission is observed ranging from the blue to near infra-red^{5,6}.

The emission from GO is widely agreed to be due to molecular-type PL associated with confined 'islands' of graphitic sp^2 regions surrounded by functionalized sp^3 regions on the GO surface⁴⁻¹³. The size of the sp^2 regions depends on the nature and amount of functionalization, which strongly affects emission energy as the molecule-like orbital energy levels around these islands changes¹⁴. Hence, the PL has been found to depend on various factors, including the functional group used^{15,16} and the degree of reduction¹⁶. In particular, contributing to

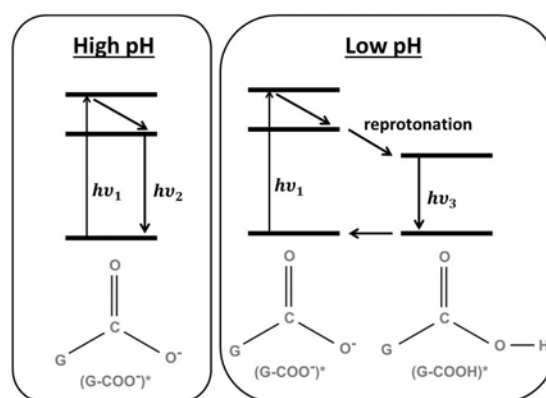


Figure 1. Schematic illustration of the photoluminescence process. At high pH, G-COO⁻ is excited to (G-COO⁻)^{*} by a photon of energy $h\nu_1$ and then relaxes to a lower lying level before emitting a photon of energy $h\nu_2$. However, at low pH, excited state reprotonation occurs forming (G-COOH)^{*}, which emits a photon of energy $h\nu_3$.

the PL are transitions associated with the -OH and -COOH groups at short and long wavelengths respectively¹². The -COOH groups are mostly deprotonated to -COO⁻ but in acidic conditions undergo reprotonation upon excitation as illustrated in Figure 1. This excited state protonation enhances long wavelength emission,

resulting in pH dependent emission bands which are commonly reported in the literature¹⁰⁻¹². The pH dependent behavior of GO can be utilized in a number of ways, but has particular use in biosensing and drug release, due to its biocompatibility and strong affinity to biological molecules such as single-strand DNA^{17,18}. This interaction is due to π - π interactions with ring structures in the nucleic acid bases¹⁹, but the conformational change associated with surface group protonation modifies the interaction and has led to the use of GO as a targeted drug delivery system²⁰⁻²³. In order to fully control this release process, a good understanding of the protonation step must be developed. This process occurs on a picosecond timescale and so ultrafast experiments are required to study it.

Previous studies of charge dynamics in GO have presented the results of PL lifetime measurements, transient absorption and femtosecond upconversion spectroscopy. These studies all show transient PL and absorption decays with a multi-exponential form, consistent with multiple populations of emitting species, which can be characterized by 3 or 4 time constants with values ranging from 0.17 ps to 1680 ps^{4,24,25}. Some pH dependent work has been reported: Zhang et al. report two bands of PL centred at 440 nm and 650 nm, with the longer wavelength band only present at lower pH levels where protonation can more readily take place¹¹; Du *et al* have detailed the concentration dependence of the pH-driven spectral shift in emission²⁶; and Konkena et al temporally resolved these spectral shifts on a nanosecond timescale²⁷. However, transient studies of the pH-dependence of GO emission have yet to be carried out with sufficient resolution to establish the timescale of the reprotonation process and thus its potential impact on the time response of its applications.

In this study we use transient absorption spectroscopy to observe and study the pH-dependent time-evolution of the protonation step in GO. This is complemented by steady state absorption and PL spectroscopy, and transient PL measurements.

2. METHODS.

A GO suspension was prepared by a 4-hour sonication-assisted exfoliation of graphite oxide powder made by a modified Hummers method. The resulting suspension was centrifuged 3 times at 8,000 rpm to remove the multilayer GO flakes. To obtain atomic force microscope (AFM) images, the graphene oxide suspension (0.1mg/mL) was diluted 1000 times and deposited onto a silicon/silicon oxide wafer (2 x 2 cm) by drop casting. The sample was dried overnight in the oven at 50 °C. The AFM measurements were carried out using Veeco Dimension 3100 under tapping mode. The data was analyzed by NanoScope Analysis software. 0.1 mg/mL GO samples with different pH value were prepared by adding KOH or HCl solutions to the GO suspension according to previous reports^{10,28}. The pH values of the suspensions were determined using a pH titration monitored by a Mettler Toledo pH meter (SevenExcellence S470 Benchtop, pH accuracy~0.001). Magnetic stirring was constantly applied to ensure the homogeneity of the dispersion. We note that there is no visible separation of graphitic material or oxidative debris as referenced by Coleman et al.²⁹ in our samples; all samples studied remain stable in suspension over many weeks.

Steady-state absorption and photoluminescence spectroscopy were performed using a Perkin Elmer Lambda 1050 UV/Vis/IR spectrophotometer and a Horiba Fluorolog-3 spectrofluorometer respectively. Excitation at 400 nm was used in the photoluminescence experiments.

Photoluminescence decay transients were obtained using time-correlated single photon counting (TCSPC). A mode-locked Ti:Sapphire (Spectra-Physics Mai Tai) generated 100 fs, 800 nm pulses at 80 MHz. The pulse rate was slowed to 4 MHz using a pulse picker (APE Pulse Select) and frequency doubled to 400 nm. TCSPC counting electronics (Edinburgh Instruments T900) were used to collect lifetime measurements for photoluminescence at 580 nm. Emission was collected via a monochromator (Horiba, SPEX 1870C) and microchannel plate (Hamamatsu R3809U-50). To ensure single photon counting, the excitation/emission count rate ratio was kept below 1%.

A broadband ultrafast pump-probe transient absorbance spectrometer (Helios, Ultrafast Systems LLC) was used to collect transient absorption data. The pump and probe beam were created by a Ti:sapphire amplifier system (Spectra Physics Solstice Ace) producing 800 nm pulses at 1 kHz with a 100 fs pulse duration. This beam was then split to form pump and probe beams. The pump portion was passed through an optical parametric amplifier (Topas Prime) to generate 300 nm excitation pulses with a FWHM (full width at half-maximum) of ~ 10 nm. The excitation beam at the sample had a beam diameter of ~ 200 μm and average power of 470 μW . The probe portion was passed through a rastered CaF_2 crystal to form a white light continuum, and absorption changes were monitored between 330–700 nm. Data was collected from -3 ps to 2 ns, with a time resolution of ± 0.22 ps, measured by the Raman response in water. Data at 600 nm is dominated by the second order diffraction of scattered pump light within the spectrometer, and so has been removed.

3. RESULTS AND DISCUSSION

AFM measurements of the GO suspension found that the lateral size (square root of the area of the flake) of the flakes varied from 0.4 to 1.2 μm . The distribution of sizes had an average of 0.75 μm and a standard deviation of 0.10 μm ; an AFM image and size histogram are given in the Supporting Information (Figure S1).

The absorbance spectra for GO colloidal suspensions under acidic and alkaline conditions are compared in Figure 2a, and shown for a range of pH values in the Supporting Information (Figure S2a). In each spectra, there is a peak at 230 nm and shoulder at ~ 300 nm associated with π - π^* transitions of C-C and C=C bonds in sp^2 regions and n - π^* of C=O bonds in sp^3 regions, respectively. While we see no significant spectral shift in these features with pH, the attenuation coefficient at wavelengths longer than 230 nm is significantly higher for basic suspensions as has been previously reported¹⁰.

In contrast to the small changes in the absorption spectrum, we observe large changes in the PL spectrum as the pH is increased, as shown in Figure 2b and in the Supporting Information (Figure S2b) for

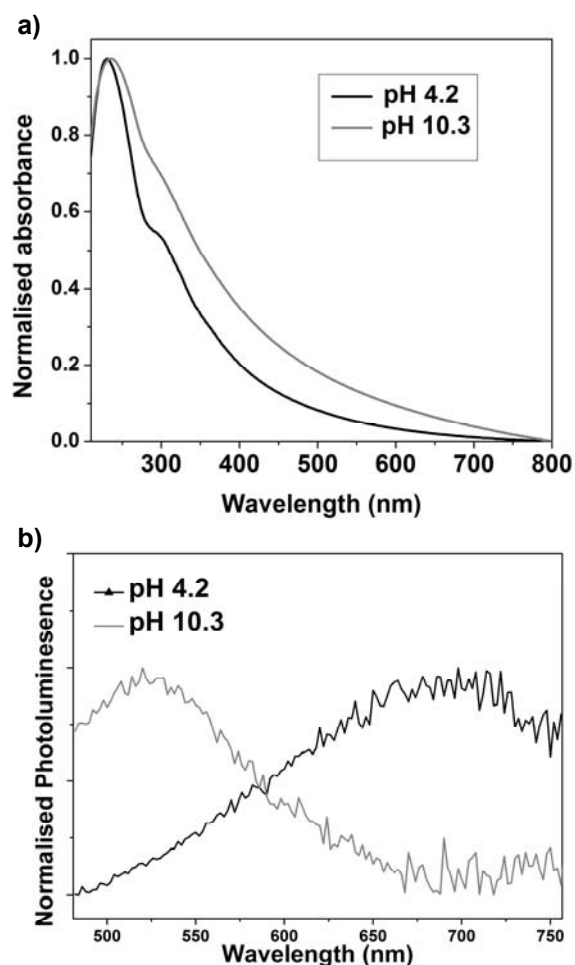


Figure 2. pH dependence of (a) absorbance spectra, normalised to the π - π^* absorbance feature at 230 nm, (b) normalised photoluminescence spectra for excitation at 400 nm.

excitation at 400 nm; an example spectrum for excitation at 300 nm is also shown in Supporting Information (Figure S3). A clear difference is seen between low (< 9.3) and high (> 9.3) pH, with broad emission bands evident centred at ~ 700 nm and ~ 520 nm, respectively. This transition between emission bands due to pH has been reported previously and is attributed to radiative recombination occurring through the $-\text{OH}$ or $-\text{COOH}$ surface groups^{10–12,30}. At high pH, a blue band arises from $-\text{OH}$ transitions, whereas in more acidic media PL is dominated by excited state transitions in the protonated $-\text{COOH}$ group, leading to a broad red emission pathway. We note that in our data the blue band may still be present below pH 9.3 but is hidden by the strong red emission, which can be seen more clearly in Figure S4. The excitation

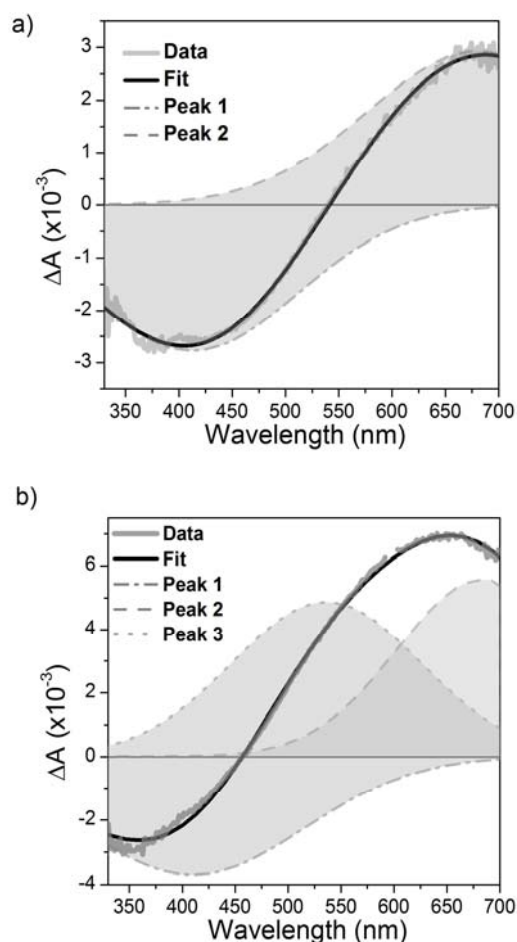


Figure 3 Differential absorption, ΔA , spectra produced by pumping at 300 nm for a pH of a) 10.2, and b) 4.2. Each spectrum is taken at its respective maximum amplitude, around 2 ps after excitation. Also shown are fits to the spectra composed of a) 2 or b) 3 Gaussian peaks.

spectra for the pH 4.2 and 9.3 samples are given in the Supporting Information (Figure S5) and broadly match the absorbance spectra in Figure 2a; there is no indication of the effect of any impurities on the photoluminescence.

To explore this phenomenon in more detail, we studied the PL lifetimes at 580 nm where both PL features have significant intensity. The resultant decay transients are shown in the Supporting Information (Figure S2b inset). At all pH values, the majority of the PL decay is very rapid and likely instrument response limited. However, for highly alkaline samples (pH > 9.3) a slower component with a lifetime of 1.8 ± 0.3 ns is seen, which is only weakly present for the other pH values. An increased PL lifetime for highly alkaline GO has been reported by Zhang et al.¹¹, although we note that our

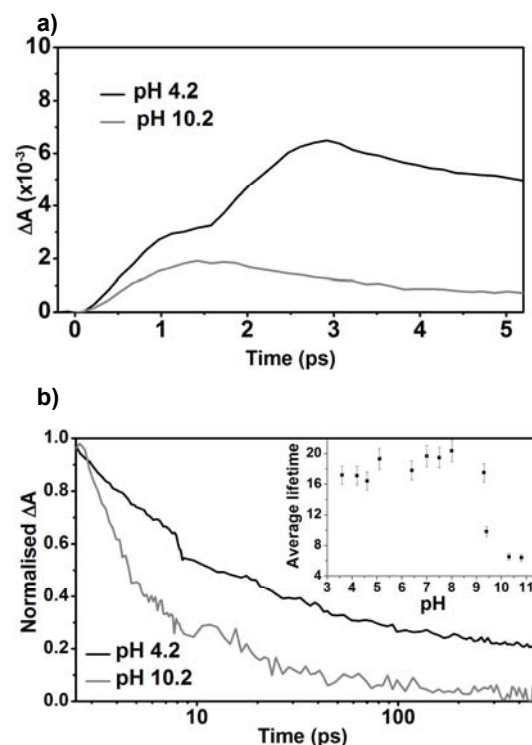


Figure 4 Differential absorption transients showing (a) stepwise growth under acidic conditions which disappears when the dispersion becomes sufficiently alkali (i.e. pH > 9.3), and (b) more rapid decay under alkali conditions. Inset: the average decay time as a function of pH.

observed emission lifetimes are shorter lived and the transition in behavior occurs at a higher pH.

These PL decay transients show that the charge dynamics occur largely on a sub-nanosecond timescale and so ultrafast transient absorption spectroscopy was used to study them further. Differential absorption, ΔA , spectra under acidic and alkaline conditions are compared in Figure 3, with spectra for a range of pH values given in the Supporting Information (Figure S6). Each spectrum is composed of a broad bleach feature at short wavelengths and photoinduced absorption feature at longer wavelengths. This latter feature is similar to that reported by Shang et al. and was attributed to excited state absorption, although they did not probe below 530 nm to the spectral region where we observe the bleach feature⁴. For pH values > 9.3, the differential spectra are well described by a fit comprising two Gaussian peaks: one (peak 1) corresponding to a bleach centred at about 400 nm and another (peak 2) corresponding to a photo-induced absorption centred at about 650 nm.

However, for pH values <9.3, the differential spectrum is described by a fit comprised of peaks 1 and 2 plus an additional photo-induced absorption centred at about 530 nm (peak 3). This pH-dependent photo-induced feature is attributed to the formation of G-COOH from G-COO⁻ via excited state protonation.

To further understand this process, its time evolution was studied. Figure 4 shows the rise and decay of ΔA at 610 nm, which will have contributions from both peak 2 and 3. There is again a stark change at pH 9.3. For pH > 9.3, the maximum ΔA is achieved at ~1.5 ps following monotonic growth. In contrast, for pH < 9.3 a stepwise growth is observed with the first step occurring over ~1.5 ps and the second also taking ~1.5 ps. This behavior is consistent with the production of an additional species whose formation is dependent on the creation of a precursor. The formation of (G-COOH)* by excited state protonation requires the initial creation of (G-COO⁻)*. The data suggests that the creation of (G-COO⁻)* occurs over the first ~1.5 ps, and is followed by a protonation step also taking about ~1.5 ps. This second process is suppressed in highly alkaline conditions and therefore this two-step process is not seen above pH 9.3.

The subsequent ΔA decay transients are shown in Figure 4b for typical acidic and alkaline dispersions, with the decays for a range of pH values given in the Supporting Information (Figure S7). The decays observed for pH>9.3 are significantly more rapid than those observed for more acidic dispersions. A similar increase in the decay rate for higher pH values has also been reported for carbon nanodots³¹. Each of the decays can be described by a triexponential function with lifetimes $\tau_1=2.0\pm 0.1$ ps, $\tau_2=15\pm 1$ ps and $\tau_3=140\pm 10$ ps, which are values similar to previous reports^{4,24,25}. However, the amplitude of component associated with τ_1 is greater for pH>9.3; this can be seen from the inset to Figure 4b which shows the average lifetime, $\bar{\tau}$, for a range of pH values. The value of $\bar{\tau}$ is calculated from the individual lifetimes weighted by the amplitude of the corresponding component; these amplitudes are given in the Supporting Information (Figure S8). The change in decay rate at pH=9.3 is consistent with the formation of a new species of functional group for pH

values less than this i.e. the excited state protonation of (G-COO⁻)* to (G-COOH)*.

In this study we see an abrupt change in behavior at pH=9.3, whereas other reports have witnessed or predicted the change at pH levels ranging from 5 to 9.5^{10,11}. This difference in the critical pH level is attributed to the sensitivity of GO's optical properties to surface functionalization which in turn depends on fabrication techniques⁷. To fully utilize this pH dependent behavior, both understanding of and control over the onset of excited state protonation must be gained.

4. CONCLUSION.

We find that the optical properties and charge dynamics of dispersions of GO undergo an abrupt change in behavior at pH 9.3. These results are consistent with the excited state protonation of (G-COO⁻), which leads to a pH dependent shift in the absorbance and PL spectra, and in the PL decay transients. This excited-state protonation also produces a broad photo-induced absorption peak centred at 530 nm. This peak exhibits stepwise growth that allows the time-scale of the protonation process to be determined as about 1.5 ps. Additionally, the recombination dynamics are affected by the onset of excited state absorption, with a increase in fast recombination pathways above pH 9.3. This understanding of the rate and effects of the protonation process will aid the exploitation of the pH-dependence of GO for applications such as biosensing and drug-release. In particular, the picosecond timescale of protonation revealed by this study means that it is very unlikely to limit the response time of applications based on GO pH-dependence.

ASSOCIATED CONTENT

Supporting information

The Supporting Information is available free of charge on the ACS Publications website.

Atomic force microscopy image and size histogram; absorbance spectra and PL spectra for excitation at 400 nm; example PL spectrum for excitation at 300 nm; PL decay transients; excitation spectra for pH 4.2 and 9.3 samples; differential absorption spectra and transients; PL decay component amplitudes.

AUTHOR INFORMATION

Corresponding Author

*E-mail: david.binks@manchester.ac.uk

Notes

The authors declare no competing financial interest.

ACKNOWLEDGEMENTS

This work was funded by the EPSRC under grants EP/L01548X/1 and EP/N010345/1. RRN and KSN are grateful to Graphene Flagship, Royal Society and European Research Council (contracts 679689 and 319277 Hetero2D). Transient absorption measurements were performed at the Ultrafast Biophysics Facility, Manchester Institute of Biotechnology, as funded by BBSRC Alert14 Award BB/M011658/1. The data associated with this paper are openly available from Mendeley data: doi:10.17632/n9tvcwccf5.1

REFERENCES

1. Novoselov, K. S.; Fal'ko, V. I.; Colombo, L.; Gellert, P. R.; Schwab, M. G.; Kim, K.. A roadmap for graphene. *Nature* **2012**, *490*, 192–200.
2. Eda, G.; Maier, S. A. Two-dimensional crystals: managing light for optoelectronics. *ACS Nano* **2013**, *7*, 5660–5665.
3. Chen, Y.; Xi, J.; Dumcencos, D. O.; Liu, Z.; Suenaga, K.; Wang, D.; Shuai, Z.; Huang, Y.-S.; Xie, L. Tunable band gap photoluminescence from atomically thin transition-metal dichalcogenide alloys. *ACS Nano* **2013**, *7*, 4610–4616.
4. Shang, J.; Ma, L.; Ai, W.; Yu, T.; Gurzadyan, G. G. The origin of fluorescence from graphene oxide. *Sci. Rep.* **2012**, *2*, 792.
5. Loh, K. P.; Bao, Q.; Eda, G.; Chhowalla, M. Graphene oxide as a chemically tunable platform for optical applications. *Nat. Chem.* **2010**, *2*, 1015–1024.
6. Eda, G.; Lin, Y.-Y.; Mattevi, C.; Yamaguchi, H.; Chen, H.-A.; Chen, I.-S.; Chen, C.-W.; Chhowalla, M. Blue photoluminescence from chemically derived graphene oxide. *Adv. Mater.* **2010**, *22*, 505–509.
7. Hasan, M. T.; Senger, B. J.; Ryan, C.; Culp, M.; Gonzalez-Rodriguez, R.; Coffey, J. L.; Naumov, A. V. Optical band gap alteration of graphene oxide via ozone treatment. *Sci. Rep.* **2017**, *7*, 1–8.
8. Zhu, S.; Song, Y.; Zhao, X.; Shao, J.; Zhang, J.; Yang, B. The photoluminescence mechanism in carbon dots (graphene quantum dots, carbon nanodots, and polymer dots): current state and future perspective. *Nano Res.* **2015**, *8*, 355–381.
9. Yang, F.; Zhao, M.; Zheng, B.; Xiao, D.; Wu, L.; Guo, Y. Influence of pH on the fluorescence properties of graphene quantum dots using ozonation pre-oxide hydrothermal synthesis. *J. Mater. Chem.* **2012**, *22*, 25471–25479.
10. Galande, C.; Mohite, A. D.; Naumov, A. V.; Gao, H.; Srivastava, A.; Weisman, R. B.; Ajayan, P. M. Quasi-molecular fluorescence from graphene oxide. *Sci. Rep.* **2011**, *1*, 85.
11. Zhang, X. F., Shao, X. & Liu, S. Dual fluorescence of graphene oxide: a time-resolved study. *J. Phys. Chem. A* **2012**, *116*, 7308–7313.
12. Cushing, S. K.; Li, M.; Huang, F.; Wu, N. Origin of strong excitation wavelength dependent fluorescence of graphene. *ACS Nano* **2014**, *8*, 1002–1013.
13. Zhao, L.; Chen, J.; He, X.; Yu, X.; Yan, S.; Zhang, S.; Pan, H.; Xu, J. Solvent induced fluorescence enhancement of graphene oxide studied by ultrafast spectroscopy. *Chem. Phys.* **2018**, *508*, 1–6.
14. Kozawa, D.; Zhu, X.; Miyauchi, Y.; Mouri, S.; Ichida, M.; Su, H.; Matsuda, K. Excitonic photoluminescence from nanodisc states in graphene oxides. *J. Phys. Chem. Lett.* **2014**, *5*, 1754–1759.
15. Vempati, S.; Uyar, T. Fluorescence from graphene oxide and the influence of ionic, π - π interactions and heterointerfaces: electron or energy transfer dynamics. *Phys. Chem. Chem. Phys.* **2014**, *16*, 21183–21203.
16. Ozcan, S.; Vempati, S.; Cirpan, A.; Uyar, T. Associative behaviour and effect of functional groups on the fluorescence of graphene oxide. *Phys. Chem. Chem. Phys.* **2018**, *20*, 7559–7569.
17. Li, X. M., Song, J., Cheng, T. & Fu, P. Y. A duplex-triplex nucleic acid nanomachine that probes pH changes inside living cells during apoptosis. *Anal. Bioanal. Chem.* **2013**, *405*, 5993–5999.
18. Salvo, P.; Calisi, N.; Melai, B.; Cortigiani, B.; Mannini, M.; Caneschi, A.; Lorenzetti, G.; Paoletti, C.; Lomonaco, T.; Paolicchi, P. et al. Temperature and pH sensors based on graphenic materials. *Biosens. Bioelectron.* **2017**, *91*, 870–877.
19. Shao, C.; Liang, J.; He, S.; Luan, T.; Yu, J.; Xu, J.; Tian, L. pH-responsive graphene oxide-DNA nanosystem for live cell imaging and Detection. *Anal. Chem.* **2017**, *89*, 5445–5452.
20. Gao, W. in *Graphene Oxide: Reduction Recipes, Spectroscopy and Applications*; Gao, W. (Ed.); Springer International Publishing: Cham, 2015, pp 61–95.
21. Wang, Y.; Li, Z.; Wang, J.; Li, J.; Lin, Y.; Graphene and graphene oxide: Biofunctionalization and applications in biotechnology. *Trends Biotechnol.* **2011**, *29*, 205–212.
22. Hashemi, H.; Namazi, H. Sonochemically synthesized blue fluorescent functionalized graphene oxide as a drug delivery system. *Ultrason. Sonochem.* **2018**, *42*, 124–133.

23. Erol, O.; Uyan, I.; Hatip, M.; Yilmaz, C.; Tekinay, A. B.; Guler, M. O. Recent advances in bioactive 1D and 2D carbon nanomaterials for biomedical applications. *Nanomedicine Nanotechnology, Biol. Med.* **2018**, *14*, 2433-2454.
24. Liu, Z.-B.; Zhao, X.; Zhang, Z.-L.; Yan, X.-Q.; Wu, Y.-P.; Chen, Y.-S.; Tian, J.-G. Ultrafast dynamics and nonlinear optical responses from sp^2 - and sp^3 -hybridized domains in graphene oxide. *J. Phys. Chem. Lett.* **2011**, *2*, 1972-1977.
25. Zhao, X.; Liu, Z.-B.; Yan, W.-B.; Wu, Y.; Zhang, X.-L.; Chen, Y.; Tian, J.-G. Ultrafast carrier dynamics and saturable absorption of solution-processable few-layered graphene oxide. *Appl. Phys. Lett.* **2011**, *98*, 121905.
26. Du, D.; Song, H.; Nie, Y.; Sun, X.; Chen, L.; Ouyang, J. Photoluminescence of graphene oxide in visible range arising from excimer formation. *J. Phys. Chem. C* **2015**, *119*, 20085-20090.
27. Konkena, B.; Vasudevan, S. Spectral migration of fluorescence in graphene oxide aqueous dispersions: evidence for excited-state proton transfer. *J. Phys. Chem. Lett.* **2013**, *5*, 1-7.
28. Lv, W.; You, C.-H.; Wu, S.; Li, B.; Zhu, Z.-P.; Wang, M.; Yang, Q.-H.; Kang, F. pH-mediated fine-tuning of optical properties of graphene oxide membranes. *Carbon* **2012**, *50*, 3233-3239.
29. Coleman, B. R.; Knight, T.; Gies, V.; Jakubek, Z. J.; Zou, S. Manipulation and quantification of graphene oxide flake size: photoluminescence and cytotoxicity. *ACS Appl. Mater. Interfaces* **2017**, *9*, 28911-28921.
30. Luo, Z.; Vora, P. M.; Mele, E. J.; Johnson, A. T. C.; Kikkawa, J. M. Photoluminescence and band gap modulation in graphene oxide. *Appl. Phys. Lett.* **2009**, *94*, 111909.
31. Sui, L.; Jin, W.; Li, S.; Liu, D.; Jiang, Y.; Chen, A.; Liu, H.; Shi, Y.; Ding, D.; Jin, M. Ultrafast carrier dynamic of carbon nanodots in different pH environments. *Phys. Chem. Chem. Phys.* **2016**, *18*, 3838-3845.

The pH Dependence of Ultrafast Charge Dynamics in Graphene Oxide Dispersions

Georgia Kime^{1,2}, Kai-Ge Zhou^{3,4}, Samantha J. O. Hardman⁵, Rahul R. Nair^{3,4}, Konstantin Sergeevich Novoselov², Daria V. Andreeva⁶, and David J. Binks^{1,2*}

¹ Photon Science Institute, University of Manchester, M13 9PL, UK

² School of Physics and Astronomy, University of Manchester, M13 9PL, UK

³ School of Chemical Engineering & Analytical Science, Univ. of Manchester, M13 9PL, UK

⁴ National Graphene Institute, University of Manchester, M13 9PL, UK

⁵ Manchester Institute of Biotechnology, University of Manchester, M13 9PL, UK

⁶ Department of Materials Science and Engineering, National University of Singapore, Singapore, 117575, Singapore

*To whom correspondence should be addressed

S1. Atomic force microscope measurements.

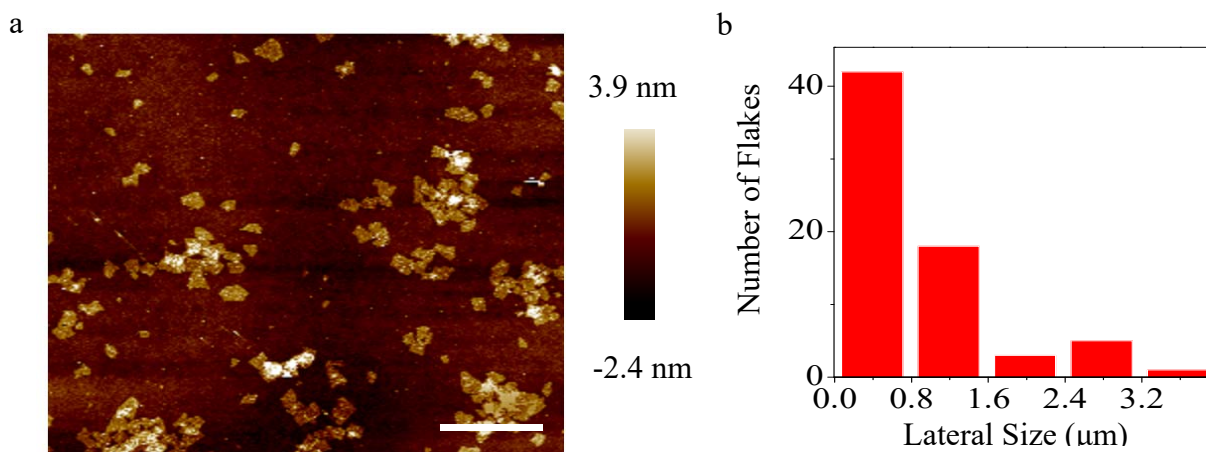


Figure S1 a) The AFM height image of as-prepared graphene oxide flakes deposited on SiO₂/Si substrate. Scale bar: 4 μ m; b) the lateral size distribution of the graphene oxide flakes. The lateral sizes of flakes were estimated by taking the square root of the area of each flake measured with the NanoScope Analysis software.

S2. Absorbance and photoluminescence spectra & photoluminescence decay transients.

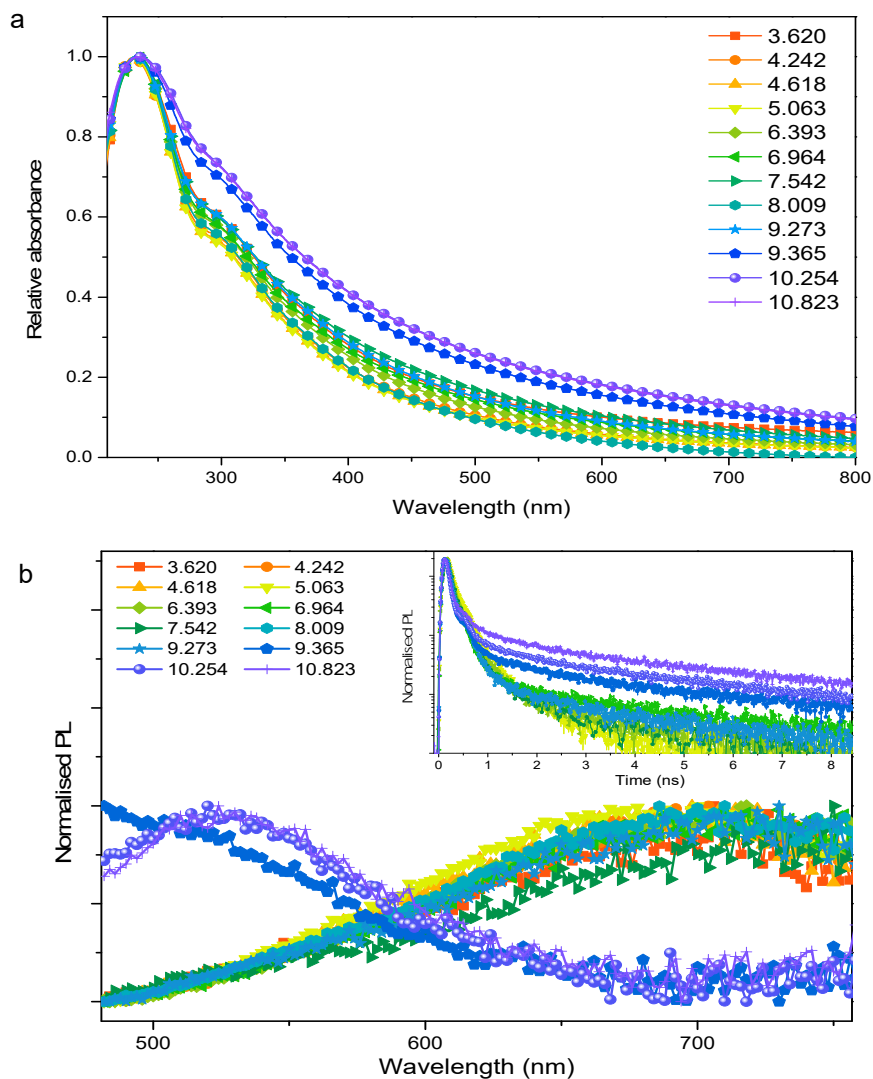


Figure S2 pH dependence of (a) absorbance spectra, normalised to the π - π^* absorbance feature at 230 nm, (b) normalised photoluminescence spectra for excitation at 400 nm, and (inset) photoluminescence transient measurements for emission at 580 nm.

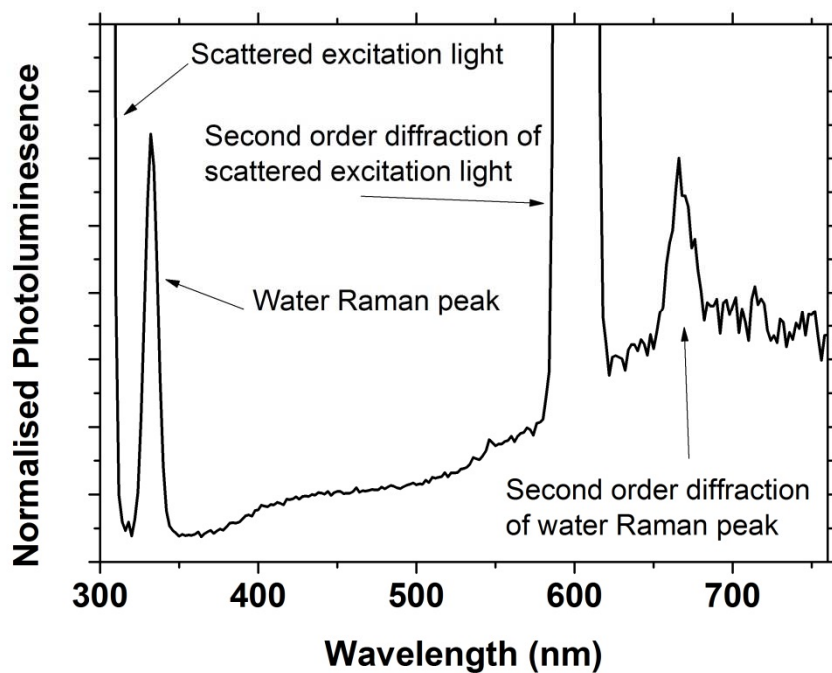


Figure S3. Spectrum for the pH=4.2 GO dispersions excited at 300 nm showing broad photoluminescence, and Rayleigh and Raman scattered excitation light that has undergone both first and second order diffraction within the spectrometer.

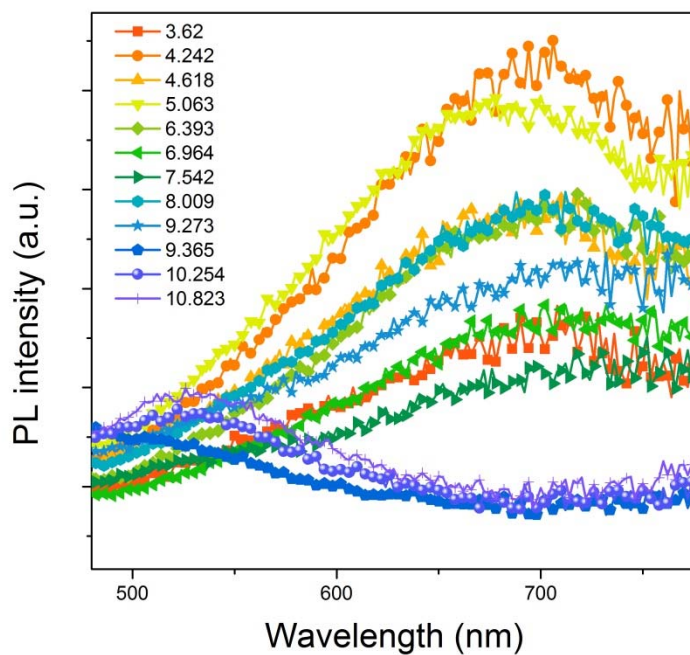


Figure S4. Steady-state photoluminescence of dispersions of GO at a range of pH levels, for excitation at 400 nm and without normalization.

S3. Excitation spectra.

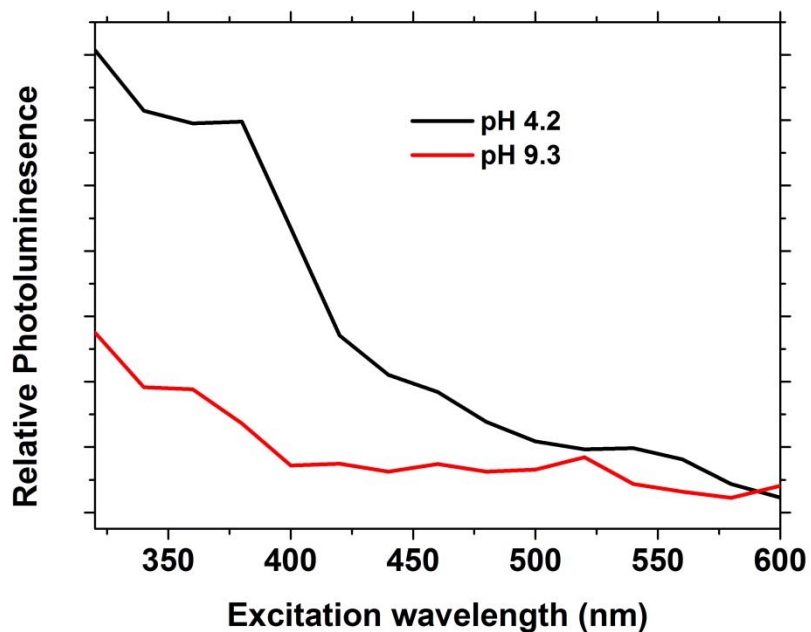


Figure S5. Excitation spectra for the pH 4.2 and pH 9.3 samples for a detection wavelength of 620 nm.

S4. Differential absorption spectra.

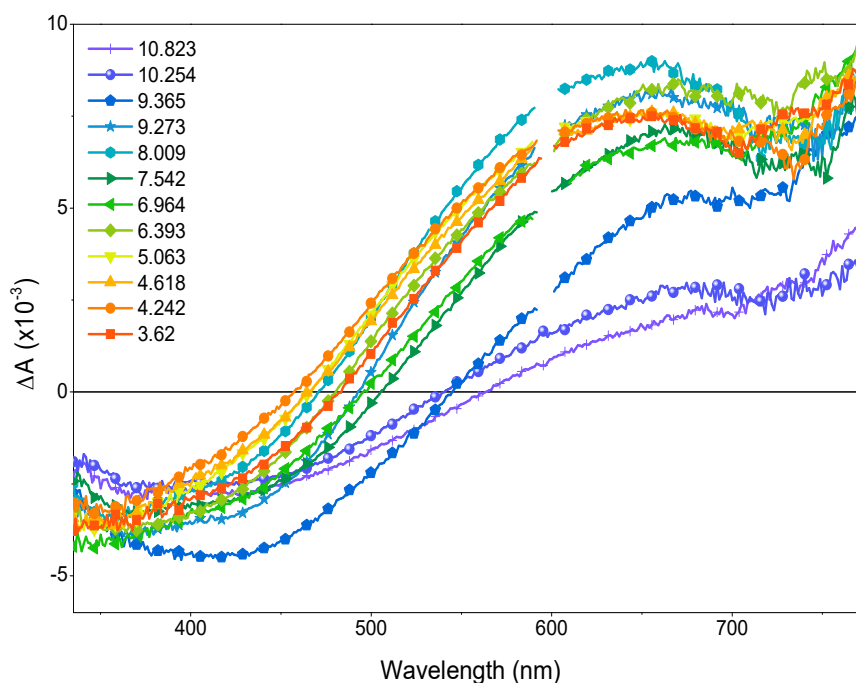


Figure S6 Differential absorption, ΔA , spectra between 330 – 750 nm following excitation at 300 nm. Each spectrum is taken at its respective maximum amplitude, around 2 ps after excitation.

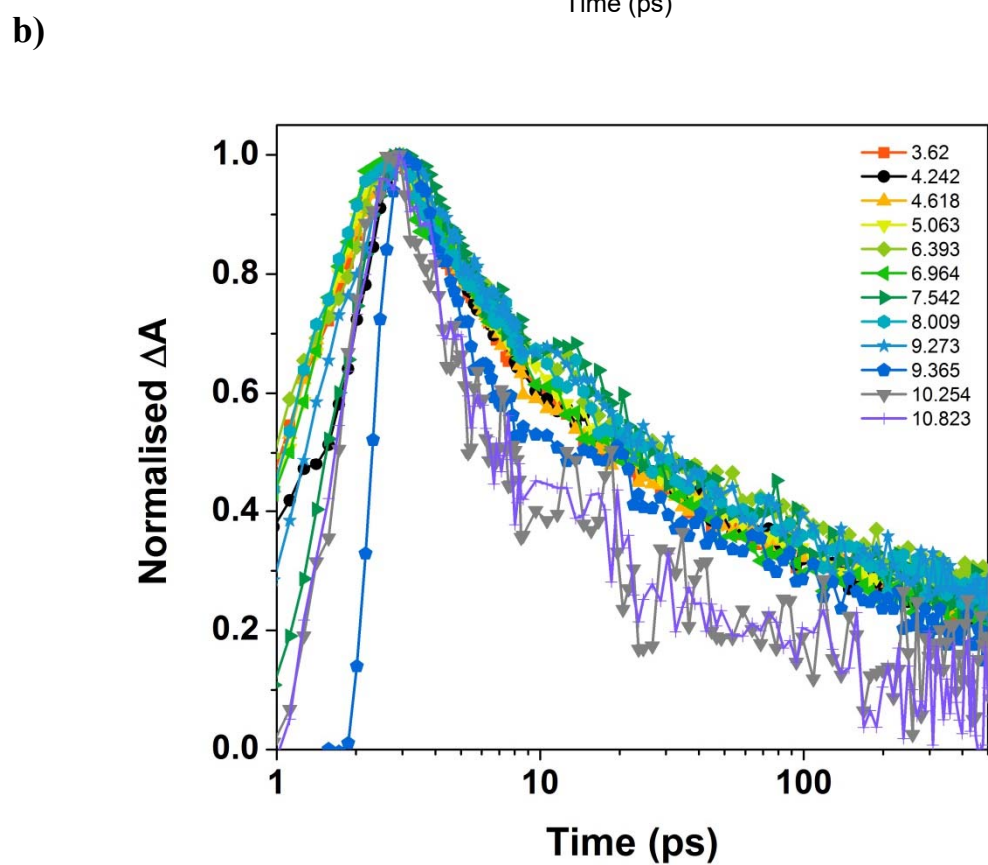
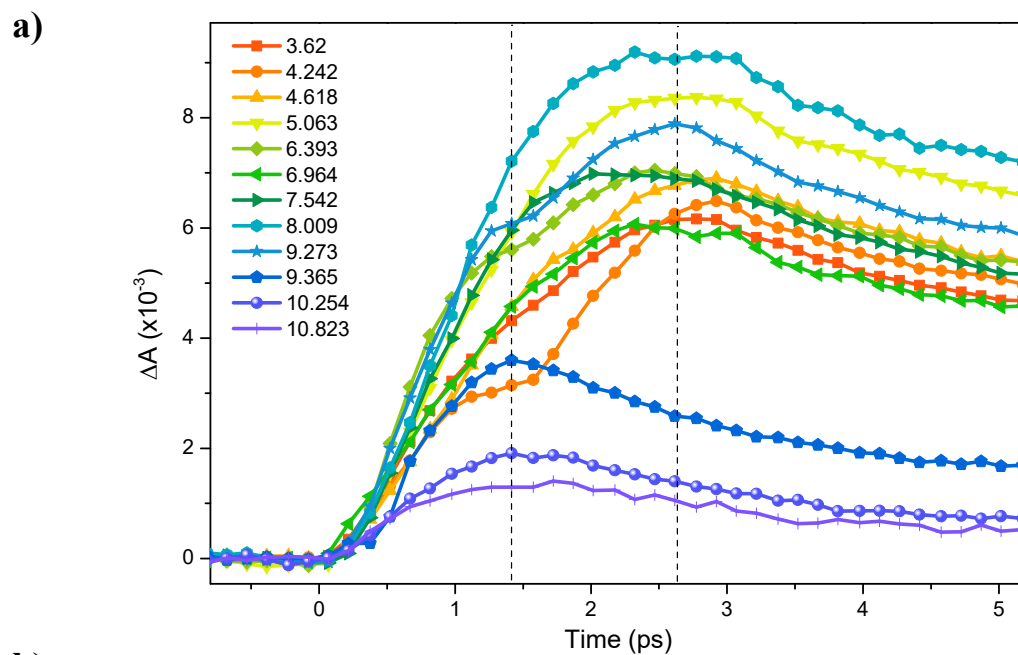


Figure S7 Differential absorption transients showing (a) stepwise growth for $\text{pH} < 9.3$ and monotonic growth for $\text{pH} > 9.3$, and (b) more rapid decay for $\text{pH} > 9.3$.

S5. Decay component amplitudes.

Globally fitting tri-exponential decays to figure 4b yields time constants $\tau_1 = 2.0 \pm 0.1$ ps, $\tau_2 = 15 \pm 1$ ps and $\tau_3 = 140 \pm 10$ ps. The variation in amplitude of each component with pH is plotted in Figure S, in which it can be seen that the amplitude associated with τ_1 increases significantly for $\text{pH} > 9.3$, with the amplitudes associated with the other time constants drops at the same point.

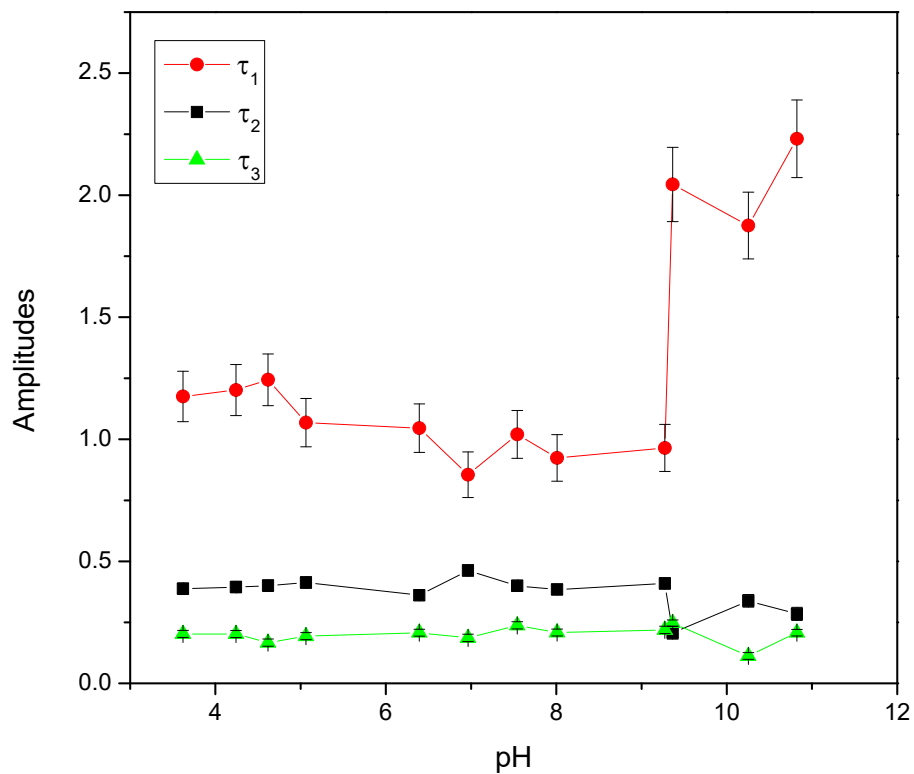


Figure S8. Amplitudes associated with the three exponential time constants (τ_1 , τ_2 , τ_3) fitted to the transient absorption decay curves of GO dispersions at a range of pH levels.